ChemPubSoc Europe

DOI: 10.1002/cctc.201501182

CHEMCATCHEM Full Papers

Influence of Microwave Irradiation on the Structural Properties of Carbon-Supported Hollow Copper Nanoparticles and Their Effect on the Synthesis of Dimethyl Carbonate

Meijiao Ren, Jun Ren,* Panpan Hao, Jinzhou Yang, Donglei Wang, Yongli Pei, Jian-Ying Lin, and Zhong Li[a]

Novel activated carbon (AC)-supported highly dispersed hollow Cu nanoparticles (NPs) (Cu/AC) with exposed {111} facets have been prepared by microwave irradiation for the synthesis of dimethyl carbonate (DMC). In particular, Cu NPs with a large cavity diameter of 35 nm are formed after irradiation from room temperature to 360 °C within a mere 8 min without additional irradiation, thus benefiting from the rapid heating of the microwave procedure. In this study, an Ostwald ripening mechanism is proposed. DFT calculations are consistent with the analysis of CO temperature-programmed desorption, which found that Cu(111) facets are more favorable for the weak adsorption of CO, which supports the formation of DMC. The as-prepared catalysts exhibit the highest DMC formation rate in terms of turnover frequency and 100% selectivity for DMC can be achieved. The large surface area of the hollow Cu NPs and the exposed {111} crystal planes are highlighted as being responsible for the excellent catalytic rate and superior selectivity, respectively.

Introduction

A revolution in the synthesis of nanomaterials has provided the opportunity to produce catalysts with controlled size and shape; this has led to the discovery that the catalytic selectivity and turnover frequency correlate with the size and shape of nanoparticles (NPs). This is referred to as "nanocatalysis".[1] In the last decade, research on hollow metal nanostructures has become prevalent because of their large surface areas, low densities, and high catalytic rates, which are superior to their solid counterparts.[2]

Despite intense efforts, it remains a significant challenge to develop facile and reliable methods for the controlled synthesis of hollow structures in terms of their size, morphology, and components. General approaches for the preparation of hollow structures have involved the utilization of various removable or sacrificial templates, including hard templates (polymers,[3] silica,[4] and metallic cores[5]) and soft templates (vesicles,[6] micelles,[7] and organic surfactants[8]). New functionalized hollow CuO nanospheres on charcoal (CuO/C) employing poly(*N*-vinyl-2-pyrrolidone) as a sacrificial template have been found to be effective catalysts under microwave irradiation because they have exhibited high reaction rates.[8g] Nevertheless, templating methods are quite tedious and costly because the process generally involves several complicated steps[3–5] and partial collapse of the hollow structures, which are the building blocks for the construction of microsized hollow structures on removing the templates. In contrast, others depend on the use of facile template-free methods, including mutual diffusion processes (known as the Kirkendall effect),[9] galvanic replacement,[10] the intermediate-crystal method,[11] hydrolysis and condensation,[12] and a reduction reaction between the core materials and reactants.[13] For instance, hollow ceria nanospheres synthesized by template-free and microwave-assisted aqueous hydrothermal methods showed an excellent adsorption capacity for heavy metal ions.[14] In CO oxidation, a 100% CO conversion is achieved at room temperature. Wang et al.[15] reported a facile and cost-effective method without using any external templates to fabricate porous hollow microstructures by a solid state chemistry based controlled decomposition–dissolution of single metal salt sources, which is particularly useful for practical industrial applications.

Dimethyl carbonate (DMC) has been utilized as an environmentally green chemical, a potential alternative to certain toxic and corrosive reagents including phosgene and dimethyl sulfide, and an oxygen-containing additive for gasoline.[16] Among the synthesis methods of DMC, there has been great interest in the vapor-phase oxidative carbonylation of methanol over supported copper-based catalysts.[16,17] Among the previously developed catalyst systems, chloride-containing Cu-based catalysts often suffer from severe deactivation because of the loss of chloride during the reaction.[18] Cu-exchanged zeolites display good efficiency for DMC synthesis with strongly enhanced

[a] *M. Ren, Prof. J. Ren, P. Hao, J. Yang, D. Wang, Y. Pei, J.-Y. Lin, Z. Li*
Taiyuan University of Technology
Key Laboratory of Coal Science and Technology
No. 79 Yingze West Street, Taiyuan 030024 (P.R. China)
E-mail: renjun@tyut.edu.cn

Supporting Information and ORCID(s) from the author(s) for this article are available on the WWW under http://dx.doi.org/10.1002/cctc.201501182.

stability.[19] However, the preparation procedure is tedious because it involves high temperatures and is time consuming. Copper(I) bromide has been dissolved in various ionic liquids for the continuous gas-phase oxycarbonylation of methanol, which has been found to be an active catalyst that increased the reaction rate and stability,[20] but halide loss through the gas stream was identified as the main reason for catalyst deactivation.

Recently, chloride-free Cu/activated carbon (AC) catalysts have been an area of significant research because the deactivation caused by chloride loss can be ultimately avoided.[21] Our previous studies have provided strong evidence for the successful introduction of highly active Cu/AC catalysts into DMC synthesis by using density functional theory (DFT) calculations[22] combined with experimental research,[21] which confirmed that it is Cu^0 that acts as the active center for DMC formation (see the Supporting Information, Figures S1 and S2). In addition, Hua et al. reported that the morphology of NPs determines the exposed crystal planes and thus significantly influences the catalytic performance.[23] Considering the excellent properties of hollow NPs, the replacement of copper solid particles by the corresponding hollow particles is suggested to provide a larger specific surface area and unprecedented catalytic performance for DMC synthesis. In addition, it remains a significant challenge to develop new catalysts with high selectivity and stability. Inspired by the thoughts of all the above, a significant improvement in the fabrication of analogous catalysts for DMC synthesis is proposed.

Herein, we have successfully produced a new series of AC-supported hollow Cu NPs catalysts by a template-free, microwave-assisted irradiation–carbothermic reduction, which makes it quite attractive for practical applications because of the rapid facile synthesis, low cost, and high selectivity. Moreover, we have studied the effects of different microwave irradiation conditions on the fine structures of the hollow Cu NPs, as well as their catalytic performance. Furthermore, the formation mechanism of such architectures and experimental results together with the corresponding theoretical calculations on the adsorption of CO on different surfaces of Cu in the rate-limiting step are also studied in detail.

Results and Discussion

Effects of reaction temperature on DMC formation rate

To assess the effect of reaction temperature on the vapor-phase oxidative carbonylation of methanol, DMC production rates were measured as a function of temperature in the temperature range 353–383 K, as shown in Figure 1 and Figure 2. The temperature was found to affect the DMC synthesis reaction very favorably; reaction rates with all materials increased with increasing temperature. In addition, a smaller difference between reaction rates is observed at lower temperatures of the temperature regime, whereas at higher temperatures, the difference in reactivity becomes larger. Notably, reaction rates with Cat-360 (NPs irradiated from room temperature to 360°C) change more rapidly compared with the others and reached

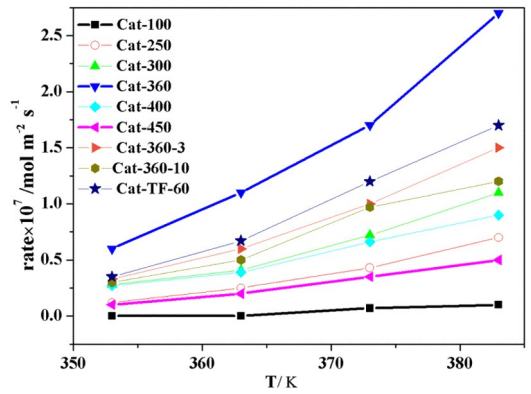

Figure 1. DMC formation rate over Cu/AC catalysts at different reaction temperatures (T = 353–383 K).

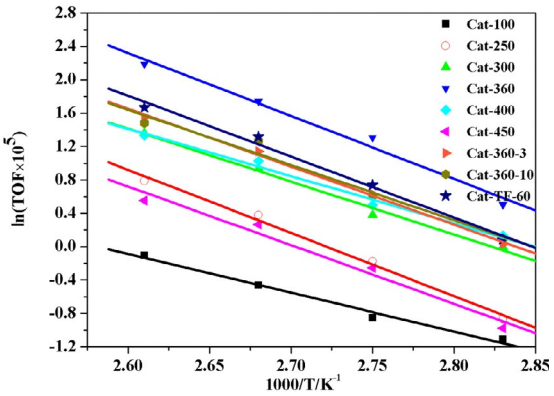

Figure 2. Arrhenius plots for the oxidative carbonylation of methanol over Cu/AC catalysts (T = 353–383 K).

a maximum of 2.7×10^{-7} mol m^{-2} s^{-1} when the temperature was 383 K, which can be attributed to the large active surface area of the hollow structures with more active sites. The corresponding apparent activation energy (E_a) and pre-exponential factor (A) were obtained from the Arrhenius plots and are shown in Table 1, with Cat-360 having a minimum $E_a = 41.5 \pm 3.8$ kJ mol^{-1}, which was less than the previously reported value of 64 kJ mol^{-1}.[24] In addition, the value of E_a was found to in-

Table 1. Kinetic parameters for the oxidative carbonylation of methanol over Cu/AC catalysts.

Catalyst	E_a[a] [kJ mol^{-1}]	A[b] [s^{-1}]
Cat-100	389.0 ± 40.2	0.05
Cat-250	158.3 ± 14.7	0.6
Cat-300	89.4 ± 9.1	3.7
Cat-360	41.5 ± 3.8	34.4
Cat-400	91.7 ± 9.5	1.5
Cat-450	166.1 ± 17.3	0.1
Cat-360-3	74.2 ± 7.1	10.8
Cat-360-10	79.2 ± 7.4	5.6
Cat-TF-60	65.8 ± 5.9	33.1

[a] Apparent activation energy. [b] Pre-exponential factor.

crease with an increase in irradiation temperature and irradiation time. Such an increase in E_a indicates that Cat-360 without additional irradiation is more favorable for the formation of DMC.

Cu/AC catalysts prepared by irradiation at different temperatures

XRD analysis

The XRD patterns of Cu/AC catalysts prepared by irradiation at different temperatures varying from 100 to 450 °C are shown in Figure 3. It is clear that when the sample is irradiated to

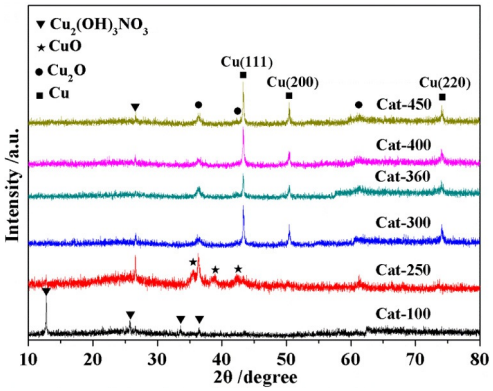

Figure 3. XRD patterns of Cu/AC catalysts obtained at different microwave irradiation temperatures.

100 °C, only diffraction peaks related to $Cu_2(OH)_3NO_3$ are detected, which implies that the precursor has not decomposed at this low temperature. As the irradiation temperature increases above 250 °C, additional peaks corresponding to CuO appear, whereas the $Cu_2(OH)_3NO_3$ peaks disappear, which can be attributed to the thermal decomposition of $Cu_2(OH)_3NO_3$ to CuO, HNO_3, and H_2O, and then, HNO_3 resolves into NO_2, O_2, and H_2O.[25] This means solid and amorphous spheres are obtained in the initial stage.[14,26] The observed main diffraction peaks at 43.3°, 50.5°, and 74.2°, which corresponded to the characteristic facets of (111), (200), and (220) of active crystalline Cu (JCPDS 65-9026), and the additional diffraction peaks of Cu_2O (JCPDS 05-0667) at 36.4°, 52.5°, and 61.3° are prominent when the temperature is elevated to 300 °C. These arise from the microwave-induced carbothermic reduction.[27] The XRD patterns at this temperature indicate that the products are mixtures of Cu and Cu_2O. Regarding the synthesis of hollow interiors, it is recognized that the ripening process may involve the mass transfer between the solid core and outer particles.[28] Note that the full width at half maximum of the Cu peaks is decreased at 360 °C, illustrating that Cu particles with smaller sizes are well dispersed on the surface of the supports.[29] Furthermore, the intensity of the diffraction peaks of Cu tend to strengthen when increasing the temperature continually, indicating that high-temperature roasting (>360 °C) may lead to active metal growth and even cause them to unite.[30]

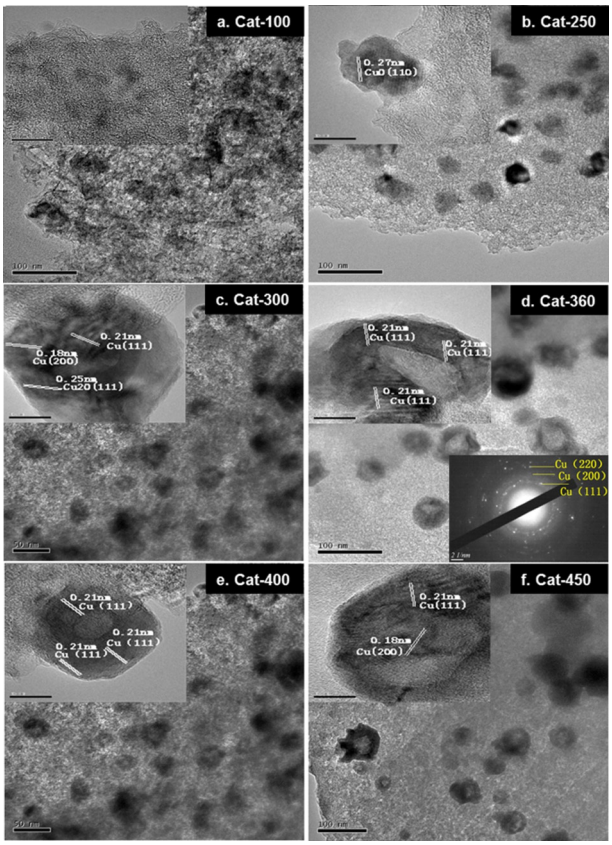

Figure 4. TEM images (insets are HR-TEM images) of Cu/AC catalysts prepared at different irradiation temperatures. The inset image in the lower right corner of (d) is the corresponding SAED pattern.

TEM analysis

As shown in Figure 4 (a–f), the TEM images reveal the interesting hollowing process of the Cu/AC catalysts prepared by irradiation to different temperatures, which are vital in illuminating the formation mechanism of the hollow NPs. On the basis of former reports, it is speculated that the Ostwald ripening process includes three stages: particles aggregates, core–shell structures, and hollow spheres.[28] It is difficult to identify clear particles in Figure 4 (a) when the irradiation temperature is 100 °C because of the undecomposed precursor. At 250 °C, owing to surface energy minimization, redistribution occurs in the process of particles mixing randomly and generating internal voids; thus, irregular particles emerge, which is the CuO phase (Figure 4 (b)) as determined by analyzing the lattice spacing. These are ascribed to the thermal decomposition of the precursors depending on the irradiation temperature. When the temperature is 300 °C, the inner core of the crystallites, which have a higher surface energy and a nanoscaled diameter, dissolves and transfers to the outside of the shells to redeposit on the better crystallized nanoparticles of the shells.[31] The sharp contrast between the dark edges and pale centers in the TEM micrograph (Figure 4 (c)) reveals the formation of hollow structures with small interior cavities, and the particles were determined to be formed of Cu_2O and Cu. When the temperature is increased to 360 °C, the solid cores are con-

sumed and disappear, forming hollow cavities inside the spheres. The surface of the AC is coated with highly dispersed and well-defined hollow structures with a large cavity, which can be confirmed as mainly Cu with exposed {111} crystal planes on determining a lattice spacing of 0.21 nm (Figure 4(d)). In its corresponding selected-area electron diffraction (SAED) pattern, the spots with a circular symmetry indicate the formation of the single-crystalline nanocopper with Cu^0 surfaces, in agreement with the XRD analysis. For Cat-400, the shell thickness increased gradually, but the {111} crystal planes were still exposed, as shown in Figure 4(e). In particular, owing to the exceptional advantage of the uniform heating of microwave irradiation, which leads to homogeneous structures of NPs,[14] the typical exposed Cu(111) crystal planes probably benefit to a great extent. Interestingly, there is a study[23] reporting that active centers that have a uniform morphology and selectively expose a single type of crystal plane are promising as highly selective catalysts. Hence, we determined that the uniform hollow Cu NPs with a high density of Cu(111) facets should be favorable for high selectivity for DMC formation.

On further raising the irradiation temperature, however, it is found (Figure 4(f)) that the cavities become irregular in shape, and some are even unclear compared with others, which is attributed to the agglomeration of nanocrystals, resulting in the distortion of the cavities owing to their extrusion into each other. Automatically, the specific active surface areas of the hollow Cu NPs and the ideal Cu(111) facets are undoubtedly reduced. This phenomenon can be clearly seen in the inset of Figure 4(f). Consequently, the conclusion can be drawn that the formation of cavities depends significantly on the irradiation temperature, and that cavities evolve initially by growing larger, then undergo irreversible distortion before finally disappearing. The optimum irradiation temperature for this process is 360 °C, which can prevent high-temperature-induced morphology changes. This conclusion is also supported by the XRD results.

CO temperature-programmed desorption (TPD) analysis

The CO-TPD profiles of the Cu/AC catalysts prepared at various irradiation temperatures are presented in Figure 5, and the Gauss–Newton curve-fitting results are given in Table 2. As depicted in Figure 5, because AC does not show any desorption properties in a control TPD spectra, the two peaks around 140 °C and 240 °C that are observed for the samples Cat-100, Cat-250, and Cat-300 can be assigned to the desorption of CO molecules interacting with the catalysts weakly and strongly, respectively.[32] When increasing the irradiation temperature to 300 °C, the intensity of the CO desorption at 240 °C decreases sharply and even becomes negligible. Correspondingly, the ratio of these two peaks increases slowly (45.4/54.6, 51.6/48.4, 62.8/37.2), and the weak CO desorption capability increases from 113.3 to 197.3. Subsequently, at 360 °C and 400 °C, only the weak desorption peak around 140 °C is observed, and the total amount of the weakly adsorbed CO on Cu decreases from 308.3 to 183.4. Of the catalysts, only Cat-360 exhibits

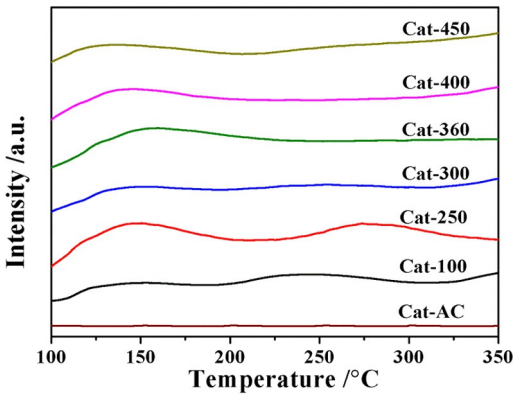

Figure 5. CO-TPD patterns of Cu/AC catalysts prepared under different irradiation temperatures.

Table 2. CO-TPD data for Cu/AC catalysts prepared at different irradiation temperatures.

Catalyst	*T* [°C]		Total area [a.u.]	Peak area ratio [%]	
Cat-AC	–	–	–	–	–
Cat-100	144.1	235.9	249.5	45.4	54.6
Cat-250	145.4	265.5	387.7	51.6	48.4
Cat-300	145.3	234.4	314.1	62.8	37.2
Cat-360	146.4	–	308.3	–	–
Cat-400	125.1	–	183.4	–	–
Cat-450	120.5	250.5	156.7	89.7	10.3

a well-resolved peak around 140 °C, which turns out to be the best desorption capability of weakly adsorbed CO (Table 2). Previous theoretical investigations indicated that CO adsorption on the Cu(111) surface is both thermodynamically favored and is a non-dissociative adsorption.[33] Thus, a preliminary summary is that the weak CO desorption capability is probably related to the selectively exposed surfaces of the Cu(111) crystal planes. However, for Cat-450, in addition to a weak desorption peak around 140 °C, a particularly weak peak around 250 °C is observed, which can be attributed to the small quantity of Cu_2O supported on the AC as the interaction between Cu^+ and CO is much stronger than that between Cu^0 and CO, as indicated in Figure S3 in the Supporting Information.

Structures and energetics of reactants absorbed on Cu(111), Cu(220), and Cu(200)

To analyze the details of the experimental results by using a theoretical approach, various possible adsorptions of CO on the Cu(111), Cu(200), and Cu(220) planes have been considered. The proposed reaction mechanism is illustrated in Scheme 1.[22] In the chemical equations, the active site is denoted by an asterisk. By analogy, the notation (Z)* indicates an active site interacting with species Z. Studies on the mechanism of DMC synthesis have shown that CO insertion into the adsorbed CH_3O to produce the adsorbed CH_3OCO species is proposed to be the rate-determining step.[22,34] Therefore, in this section, the adsorption energy (E_{ads}), activation barriers,

$1/2O_2 + * \rightarrow O*$, (1)
$CH_3OH + * \rightarrow (CH_3OH)*$, (2)
$(CH_3OH)* + O* \rightarrow CH_3O* + OH*$, (3)
$(CH_3O)* + CO \rightarrow (CH_3OCO)*$, (4)
$(CH_3OCO)* + (CH_3O)* \rightarrow (DMC)*$, (5)
$(DMC)* \rightarrow DMC + *$. (6)

Scheme 1. The proposed mechanism of DMC formation by oxidative carbonylation of methanol.

and reaction energies of the CO insertion reaction on different crystal planes of Cu are discussed, and the corresponding results are summarized in Figure 6 and Table 3. Here, the adsorption energy is used to characterize the strength of CO bonding on the Cu surfaces and is defined as $E_{ads} = E(CO/Cu) - E(Cu) - E(CO)$, where $E(CO/Cu)$ is the total energy for Cu with the adsorbed CO on the surface, $E(CO)$ is the total energy of free CO, and $E(Cu)$ is the total energy of the bare slab of the surface. The selected optimized configurations of the reactants, transition states (TSs), and products involved in Equation (4) are shown schematically in Figure 7.

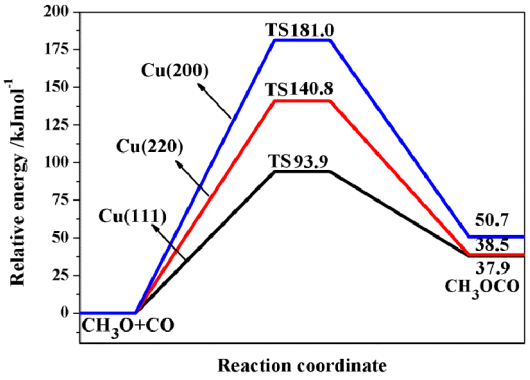

Figure 6. Energy profiles with the energy values involved in the reaction of CO insertion to methoxide species on different Cu surfaces.

Table 3. The adsorption energies of reactants and intermediates adsorbed on different surfaces.

Species	E_{ads} [kJ mol^{-1}]		
	Cu(111)	Cu(220)	Cu(200)
CO	−81.6	−95.0	−101.3
OCH_3	−256.2	−268.0	−267.5
CH_3OCO	−175.6	−198.7	−203.2

It was found that the crystal plane is very sensitive to these thermodynamic parameters. By comparison, the binding of the CO molecule to the Cu(111) surface is found to be distinctly weaker ($E_{ads} = -81.6$ kJ mol^{-1}) than to Cu(220) ($E_{ads} = -95.0$ kJ mol^{-1}) or Cu(200) ($E_{ads} = -101.3$ kJ mol^{-1}), as shown in Table 3. Nevertheless, the weakly adsorbed CO can decrease the activation energy for further reaction. Interestingly, Cu(111) (93.9 kJ mol^{-1}) alone can reduce the activation barrier compared with Cu(220) (140.8 kJ mol^{-1}) and Cu(200) (181.0 kJ mol^{-1}), giving an insertion reaction that is endothermic and follows the order Cu(111) (37.9 kJ mol^{-1}) < Cu(220) (38.5 kJ mol^{-1}) < Cu(200) (50.7 kJ mol^{-1}), indicating that Cu(111) is the most favorable for the process. In other words, the geometries of the weak interaction modes for CO on the Cu(111) facets are thermodynamically favored, which is responsible for the formation of DMC. These results fit quite well with the previous experimental observations.

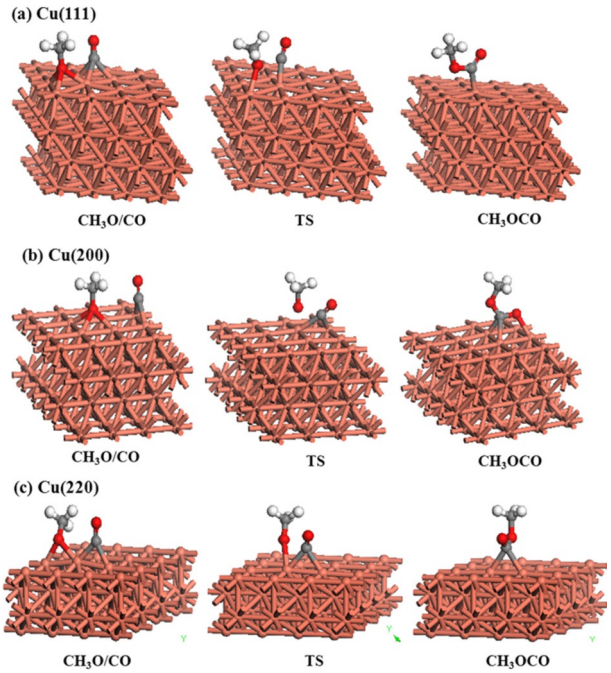

Figure 7. Optimized co-adsorbed structures and transition states on different Cu surfaces of Cu^0/AC involved from Equation (4). Dark orange balls represent Cu atoms, red balls represent O atoms, gray balls represent C atoms, and white balls represent H atoms throughout this study.

Catalytic test results

The catalytic results with the catalysts synthesized by irradiation to different temperatures are presented in Table 4. It was observed that as the irradiation temperature increases from 100 °C to 360 °C, the conversion of CH_3OH (C_{CH_3OH}), the selectivity (S_{DMC}), turnover frequency (TOF), and rate for DMC formation increase remarkably (i.e., from 2.0 to 5.8%, 78.4 to 100%, 0.9 to 8.4×10^{-5} s^{-1}, and 0.1 to 2.7×10^{-7} mol m^{-2} s^{-1}, respectively) and reach a maximum value at 360 °C, then decline dramatically beyond that point. As expected, Cat-360 shows the highest TOF value of 8.4×10^{-5} s^{-1}. To justify the good catalytic performances of Cat-360, the observed rate was compared with reported values; Li et al. reported a production rate for DMC of 229 mg g^{-1} h^{-1} over Cu/AC at 393 K,[35] Ma et al.[36] achieved the best production rate of 117 mg g^{-1} h^{-1} on Cu_2O/AC at 413 K, and 3.8×10^{-5} s^{-1} was reported over a Cu^+Y zeolite by Bell and Zhang at 403 K.[34] Importantly, all these values were obtained with more severe reaction conditions than those used with Cat-360. Thus, it appears that the hollow structure NPs in this study are more conducive to the reaction than solid ones. Additionally, the S_{DMC} of Cat-360 is up to

Table 4. Results of chemisorption and intrinsic catalytic synthesis over various Cu/AC catalysts prepared at different irradiation temperatures.

Catalyst	d_{Cu} [nm][a]	d_{Cu} [nm][b]	d_{Cu} [nm][c]	Cu dispersion (D_{Cu}) [%][d]	S_{Cu} [$m^2 g^{-1}$][e]	C_{CH_3OH} [%]	S_{DMC} [%]	STY [$mg g^{-1} h^{-1}$]	Rate($\times 10^7$) [$mol m^{-2} s^{-1}$][f]	TOF($\times 10^5$) [s^{-1}]
Cat-100	–	–	–	0.5	0.7	2.0	78.4	81.1	0.1	0.9
Cat-250	–	–	–	1.2	1.3	2.6	82.2	280.2	0.7	2.2
Cat-300	35.7	20.5	34.1	7.8	9.2	3.5	87.1	333.1	1.1	3.9
Cat-360	51.4	34.6	50.0	10.5	15.7	5.8	100.0	596.9	2.7	8.4
Cat-400	55.1	39.2	53.9	6.1	7.4	2.6	100.0	303.6	0.9	3.8
Cat-450	67.6	49.3	65.3	3.6	5.3	2.2	80.9	253.3	0.5	2.1
Cu/AC[35]	12.0	8.0	11.0	8.9	2.4	9.2	59.3	229	–	–
Cu_2O/AC[36]	–	–	–	–	–	9.2	61.0	117	–	–
Cu^+Y zeolite[34]	–	–	–	–	–	–	85.0	–	–	3.8

[a] Average particle size determined by TEM. [b] Determined by N_2O chemisorption from Equation (10). [c] Calculated from the Cu(111) plane by using Scherrer equation and XRD data. [d] D_{Cu} = the amount of exposed Cu on the surface of the catalysts from Equation (9). [e] The specific copper surface area determined by N_2O chemisorption calculated from Equation (8). [f] DMC formation rate.

100%; moreover, no byproducts are detected. In addition, Cat-360 shows a much higher C_{CH_3OH} value than the other five samples, which are all less than 4%. It is believed that C_{CH_3OH} is dependent on the amount of surface Cu atoms.[37] Interestingly, the 100% selectivity is remarkably higher than any previously reported values, with the exception of that obtained on the CuCl/MCM-41 catalyst by Li et al.[38]

Combining the results of XRD, TEM, CO-TPD, and the DFT calculations stated above, it is clear that the significant variations of TOF (and rate) for DMC formation depend strongly on the increased specific surface area of the hollow Cu structures possessing the largest cavity, which provides more available active centers for the reactants. Regarding the high selectivity for DMC, this can be attributed to the adequately exposed Cu(111) crystal planes that are identified as the catalytically active sites for the production of DMC under the optimal conditions of microwave irradiation.[22,39]

In addition, it is suggested that the Cu(111) crystal planes are dominant for the weak adsorption of CO around 140 °C rather than the intense peak around 240 °C, which is probably related to Cu_2O species, hindering the formation of the methoxide species and thus the formation of DMC;[32a] this further inhibits the side reactions and hence improves the selectivity for DMC. Interestingly, note that the sequence of increasing surface concentration of weakly adsorbed CO on the functioning catalysts is in the order Cat-360 > Cat-300 > Cat-400 ≈ Cat-250 > Cat-450 ≈ Cat-100, in line with the observed sequences for TOF and selectivity of DMC. Therefore, we strongly believe that the exposed Cu(111) facets can be identified as the best adsorption sites for the weak adsorption of CO. Coincidentally, the preferential adsorption further determines the higher selectivity of the catalyst for the oxidative carbonylation of methanol, and the TOF_{DMC} also is enhanced accordingly.

Cu/AC catalysts prepared at different retention times

XRD analysis

XRD patterns of Cat-360 synthesized with different retention times, Cat-360-0, Cat-360-3, and Cat-360-10, are displayed in Figure 8. For this, the catalysts were heated from room temperature to the desired irradiation temperature, which was then held for 0, 3, or 10 mins. The diffraction peaks centered at $2\theta = 43.3°$, 50.5°, and 74.2° are attributed to crystalline Cu (JCPDS 65-9026), whereas the weak and broad diffraction peaks located at $2\theta = 36.3°$, 42.2°, and 61.2° (JCPDS 05-0667) can be assigned to crystalline Cu_2O, indicating that the copper species have undergone the transformation from precursor to copper oxide and then to metallic Cu and Cu_2O under the microwave-induced carbothermic reduction at 360 °C.[25a,27] In addition, the intensity of the Cu species becomes sharper with increasing reaction time, indicating that the metal particles grow and even aggregate in the form of micro-crystals in this situation.[27c] Hence, the decreasing specific surface area is partially attributed to the increase in crystalline Cu.[19c] The average outside diameters of Cat-360-0, Cat-360-3, and Cat-360-10 are 50.0, 53.6, and 57.6 nm, respectively, calculated by using the Debye–Scherrer equation. It is clear that the sizes of the catalysts show a considerable increase on increasing reaction time, implying the coalescence of partial particles. This indicates that the retention time has a significant influence on controlling the crystallite growth, which further affects the textural structure and specific surface area.

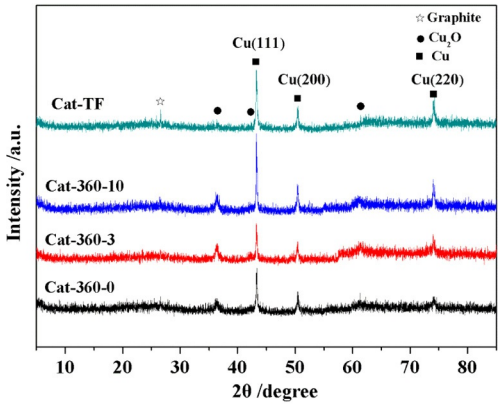

Figure 8. XRD patterns of Cu/AC catalysts prepared at different irradiation times.

TEM analysis

The microstructures of Cat-360 at different reaction times were further studied by TEM, as shown in Figure 9(a–c). For all three samples treated by microwave irradiation, the surface of the catalysts is covered with hollow metal particles majorly comprising Cu(111) and to a lesser extent Cu_2O(111). In the case where the temperature was not held at 360 C for any significant time (Cat-360-0), hollow structures with the largest cavity of approximately 35 nm diameter were formed; moreover, certain "open-mouth hollow spheres" are also present, as indicated by the black arrows in Figure 9(a), and in the inset, a high-magnification image of an individual open-mouth sphere clearly shows that the opened sphere is hollow, which increases the specific surface area for reactants to some extent. When the catalysts are collected after 3 min, in addition to some hollow metal particles with a smaller cavity of 15 nm, solid particles start to emerge. As the irradiation duration is extended to 10 min, the quantities of solid particles increase significantly, whereas the hollow structures become almost ambiguous, and noticeable distortion occurred unexpectedly (Figure 9(c)) because of serious aggregation and sintering of Cu particles. In contrast, in the catalysts roasted by the conductive heating method, Cat-TF-60, it is very difficult to find any hollow particles (Figure 9(d)), and the irregular solid particles are approximately 42.5 nm in size based on 50 particles randomly selected. The corresponding SAED pattern shows concentric diffraction rings, indicating the polycrystalline nature of the sphere (Figure 9(d)). All rings can be indexed to the diffractions from Cu_2O and Cu^0. These results agree well with the XRD patterns mentioned above. In summary, the size of the cavity and specific surface area of hollow Cu NPs can be effectively controlled by varying the irradiation time.

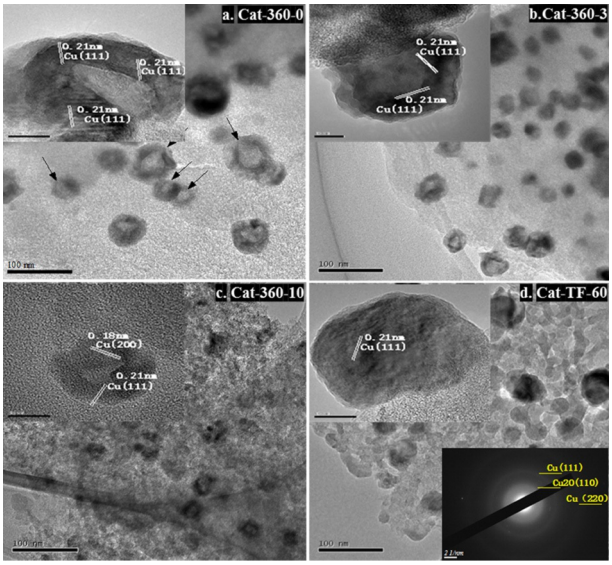

Figure 9. TEM images (insets are HR-TEM images) of Cu/AC catalysts prepared with different irradiation times and Cu/AC catalyst roasted in a tubular furnace (d; inset is the HR-TEM image and corresponding SAED pattern).

Catalytic test results

As shown in Figure S4 and Table S1 (in the Supporting Information), the AC was dominated by micropores, implying the micropore structure is not blocked by Cu nanoparticles. Therefore, the as-prepared supported catalysts with porous channels can ensure high permeation and mass-transfer rates for species involved in a catalytic reaction. It is clearly observed that for Cat-360, increasing the irradiation time leads to a remarkable decrease of more than 47% of the TOF_{DMC}, from 8.4 to 4.4×10^{-5} s^{-1}; simultaneously, the values of both C_{CH_3OH} and S_{DMC} substantially decrease from 5.8 to 3.2% and from 100 to 80.2%, respectively, as demonstrated in Table 5. This behavior corresponds well with the morphology-dependent catalytic selectivity of the hollow nanocrystals.[23] On the basis of the results of XRD and TEM, the time taken for microwave irradiation has a tremendous effect on the development of hollow structures and volume sizes, which in turn affect the active surface areas, further determining the catalytic performance. Meanwhile, the amount of exposed Cu(111) crystal planes is also affected, which relatively sensitively affects the catalytic selectivity.[22] Moreover, the catalysts roasted by the tubular furnace barely have any hollow particles, so express lower reaction rates and selectivity for DMC than the optimal catalyst irradiated by a microwave oven; this further highlights the advantages of the microwave oven, especially the characteristic of the quick rundown of irradiation temperature.

The formation mechanism of hollow copper nanostructures

On the basis of the analytical results of XRD and TEM, a possible mechanism for the formation of hollow Cu nanostructures is proposed, as illustrated in Scheme 2.

Primarily, the outer layer of $Cu(NO_3)_2$ is decomposed in situ to produce CuO nanostructures under vacuum without any significant collapse. Subsequently, almost all the CuO particles are immediately reduced in situ to produce a high concentration of Cu and are surrounded by Cu(111) crystal planes because of the microwave-induced carbothermic reduction when the temperature is above 300 °C.[27a,b] These are deposited on the surface of the precursor, forming a thin discontinuous metal shell, which allows the out-diffusion of the inner particles. The precursor inside failed to decompose because of the large temperature difference between the inside and outside, thus leading to the formation of $Cu(NO_3)_2$@Cu core–shell structures. The core begins to continually pyrolyze depending on thermal conduction, wherein the released gas[40] and excess Gibbs free energy stored in the amorphous structure work as the driving force for the outward diffusion of the core species,[41] leading to a continual decrease in the core size, and eventual depletion accompanied by the well-known inside-out Ostwald ripening process.[42] Therefore, the internal precursors acted as the cores and are considered as sacrificial templates in the formation of the hollow structure. As the reduction and decomposition proceeded, the decomposed materials originating from the cores constantly attached to the previously formed shells and are subsequently reduced to low-valent

Table 5. Results of chemisorption and intrinsic catalytic synthesis over various Cu/AC catalysts prepared with different irradiation times.

Catalyst	d_{Cu} [nm][a]	d_{Cu} [nm][b]	d_{Cu} [nm][c]	Cu dispersion (D_{Cu}) [%][d]	S_{Cu} [$m^2 g^{-1}$][e]	C_{CH_3OH} [%]	S_{DMC} [%]	Rate($\times 10^7$) [$mol\,m^{-2}\,s^{-1}$][f]	TOF($\times 10^5$) [s^{-1}]
Cat-360-0	51.4	34.6	50.0	10.5	15.7	5.8	100	2.7	8.4
Cat-360-3	54.3	38.7	53.6	6.3	10.4	3.3	80.2	1.5	4.7
Cat-360-10	60.1	43.1	57.8	2.9	9.9	3.2	81.5	1.2	4.4
Cat-TF-60	42.5	23.9	40.7	8.4	11.5	3.6	79.3	1.7	5.3

[a] Average particle size determined by TEM. [b] Determined by N_2O chemisorption from Equation (10). [c] Calculated from the Cu(111) plane by using Scherrer equation and XRD data. [d] D_{Cu} = the amount of exposed Cu on the surface of the catalysts from Equation (9). [e] The specific copper surface area determined by N_2O chemisorption calculated from Equation (8). [f] DMC formation rate.

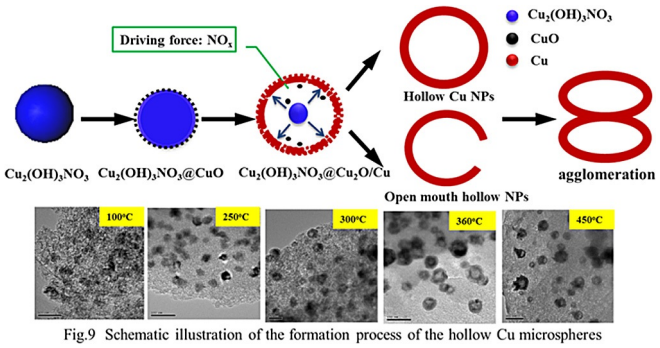

Fig.9 Schematic illustration of the formation process of the hollow Cu microspheres

Scheme 2. Schematic of the Ostwald-ripening-coupled self-assembly process of the hollow Cu structures.

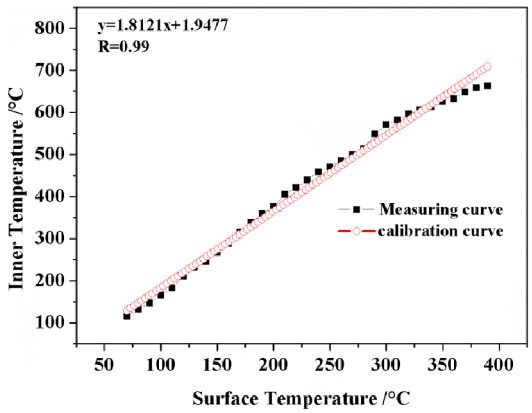

Figure 10. Microwave calibration curve.

metal species; finally, a compact metal shell is fabricated.[14] In this manner, various metal nanostructures with hollow interiors can be perfectly synthesized.

Interestingly, the features of the "open-mouth hollow spheres" in the inset of Figure 9(a) can be observed for some copper NPs, further indicating that the NPs are actually hollow spherical structures. As for the formation of fresh holes in the shell, conventionally, it can be interpreted as follows. Because oxide grows over the perimeter of metal precursors up to a certain critical thickness and then expands in size through a gradual process, the shape of the void is related to the initial shape of the metal precursors,[43] which acts as a so-called template for creating the shape of the void.[15] Note that the voids of the hollow copper structures are generally not spherical. Thus, compressive stress builds up because of the internal thermal decomposition of the precursors, and the released gas expands, which causes strong propulsion, leading to size expansion. Furthermore, the hollow interior, particularly with a non-spherical void and thin shell, is neither energetically favorable nor has sufficient mechanical strength to sustain the internal pressure compared with the external vacuum environment. These reasons might contribute to the instability of hollow copper NPs and the breakage of cavities.[44] Specifically, if annealing is performed immediately when the temperature reaches the desired value of 360 °C, the morphology of the cracked hollow structures would be retained to form stable holes, utilizing the advantage of the microwave not having thermal inertia, which is not possible in the conductive heating method.

Notably, such stable, hole-like microspheres display a perfect catalytic rate of DMC production compared with other samples, ascribed in part to the large specific surface area and the exclusive exposed Cu(111) crystal planes, which provide more access for the catalytic reaction. Therefore, to some extent, one can envisage that such structural characteristics as high-energy facets and high surface area are propitious to the formation rate and selectivity of the target product.

Conclusions

The development of catalysts with high selectivity and formation rate for DMC synthesis has been achieved for the first time. The optimal sample characterized for the hollow copper NPs has large cavities of approximately 35 nm diameter and 50 nm outside diameter, it is well dispersed on the AC support, and is rapidly fabricated by heating the precursor from room temperature to 360 °C within a mere 8 min in a special microwave heating system. A high TOF_{DMC} value of $8.4\times10^{-5}\ s^{-1}$ with C_{CH_3OH} of 5.8% and 100% S_{DMC} are obtained, which are much better than the previously reported Cu–zeolites or AC-supported copper catalysts. Notably, the attractive catalytic performance of the Cu/AC catalysts is attributed to the high surface area of the hollow copper NPs, whereas the excellent selectivity for DMC can be attributed to the completely exposed Cu(111) crystal planes. DFT calculations show that the adsorption energy of CO on Cu(111) ($-81.6\ kJ\,mol^{-1}$) is weaker

than that on Cu(220) and Cu(200), which contributes to the weak adsorption of CO and further formation of DMC.

The formation mechanism of the novel hollow copper microstructures can be elucidated by Ostwald ripening, wherein the initial stage is the aggregation of primary NPs collected by the decomposition of $Cu(NO_3)_2$, followed by the hollowing of the core and the progressive redistribution of matter from the interior to exterior. Finally, a hollow architecture is obtained by self-assembly under microwave-induced carbothermic reduction. Unexpectedly, the volume of the cavity is reduced and disappears completely at an elevated irradiation temperature or a prolonged reaction time, which gives rise to a corresponding decline in the formation rate and selectivity of DMC.

Experimental Section

Materials

Copper nitrate ($Cu(NO_3)_2{\cdot}3H_2O$) was purchased from Sinopharm Chemical Reagent Co., Ltd. AC is a commercial product obtained from Xinhua Chemical Plant (Taiyuan, China). Quartz sand used for all experiments was obtained from Tianjin Guangfu Technology Development Co., Ltd. All chemicals were of analytical grade and used without any further purification.

Preparation of Cu/AC catalysts

In a typical synthesis, $Cu(NO_3)_2{\cdot}3H_2O$ (2.4 g) was dissolved in deionized water (4.5 mL). The homogeneous solution was impregnated dropwise into AC (3.2 g, >200 mesh) and then placed in a 70 °C water bath for 12 h. Subsequently, the mixture was kept in air at 70 °C for 12 h and then at 90 °C for 12 h.[21] Finally, the precursor was placed in an NJZ4-3 microwave experimental setup (Nanjing Jiequan Microwave Equipment Co., Ltd., Nanjing, China) for irradiation at different temperatures and times under a vacuum of −0.05 MPa, and then, the Cu/AC catalysts with a Cu loading of 16.7 wt% were obtained.

The temperature in the microwave oven was measured by an infrared radiation thermometer and then corrected by a K-type thermocouple. The detailed temperature linear calibration procedure was as follows. The precursor prepared herein was irradiated at a heating rate of approximately 48 °C min^{-1} to 450 °C under a relatively low power of approximately 320 W, and, simultaneously, the temperature was recorded at an interval of 10 °C based on the surface temperature; the surface temperature of the catalyst was measured by an infrared thermometer. The inside temperature was determined by using a K-type thermocouple and is denoted as the inner temperature. The temperature calibration curve is shown in Figure 10. The Cu/AC catalysts irradiated at 100, 250, 300, 360, 400, and 450 °C corresponded to sample inner temperatures in the microwave oven of 183, 455, 545, 654, 727, and 817 °C, respectively, and were denoted as Cat-100, Cat-250, Cat-300, Cat-360, Cat-400, and Cat-450. The catalysts irradiated at 360 °C for 0, 3, or 10 min were denoted as Cat-360-0, Cat-360-3, and Cat-360-10, respectively. Thus, Cat-360 is the same sample as Cat-360-0. For comparison, the catalyst heated in a GSL-1500X tubular furnace (Hefei Kejing Materials Technology Co., Ltd., Hefei, China) at 360 °C in a 10% H_2/N_2 mixture for 60 min was designated as Cat-TF-60.

Characterization technologies

X-ray diffraction (XRD) data were recorded by using an X-ray diffractometer (D/Max 2500, Rigaku Industrial Co., Tokyo, Japan) with a CuK_α radiation source ($\lambda = 1.54056$ Å) and a graphite monochromator (operating at 40 kV and 100 mA). The range of the spectral scan (2θ) was 10°–80° and was obtained at a rate of 8° min^{-1}.

Transmission electron microscopy (TEM) and selected-area electron diffraction (SAED) were performed by using a Hitachi H-800 transmission electron microscope operating at 200 kV. The samples for TEM measurements were prepared by dispersing the products in ethanol by using an ultrasonic bath for 10 min, and then, a drop of the suspension was placed on a carbon-coated copper grid at room temperature.

CO temperature-programmed desorption (CO-TPD) was performed by using a Finsore-3010 apparatus (Zhejiang FINETEC). A sample (50 mg, >200 mesh) was placed in a U-shaped quartz tube and then heated at 10 °C min^{-1} to 300 °C under a stream of He (20 mL min^{-1}) for 1.5 h. Subsequently, the sample was cooled to ambient temperature. To saturate the catalyst, a CO stream (20 mL min^{-1}) was injected into the reactor for 60 min. Thereafter, the sample was swept with helium to remove the physically absorbed carbon monoxide. After purging the sample, the furnace temperature was increased to 600 °C at a heating rate of 10 °C min^{-1} under a helium flow.

N_2O pulse chemisorption[45] of the catalysts was performed by using a Micrometrics AutoChem II 2920. First, the sample (100 mg) was placed in a U-shape quartz reactor and each catalyst was reduced at 450 °C in a 10% H_2/Ar mixture for 60 min. Then, the reactor was purged with N_2 at 50 °C. Subsequently, N_2O was used to oxidize surface copper atoms to Cu_2O (s). The specific surface area of Cu was calculated by dissociative N_2O adsorption on the surface of copper with the pulse titration method based on Equation (7):

$$2\,Cu(s) + N_2O \rightarrow N_2 + Cu_2O(s) \quad (7)$$

Additionally, a filter filled with soda lime for trapping acidic gas N_2O was employed. The evolution of N_2 was analyzed by using a thermal conductivity detector (TCD) to detect the consumption of N_2O (X) with 1×10^{19} atoms m^{-2}. The value of $d_{average}$ in nanometers was calculated by assuming a spherical particle shape. The active copper surface areas ($m^2\,g_{Cu}^{-1}$), copper metal dispersion (%), and average copper particle size (nm) were calculated from Equations (8)–(10), respectively:

$$S_{Cu} = \frac{2XN_A a}{1\times10^{19}\times(1+a)} \quad (8)$$

$$D_{Cu} = \frac{2X(1+a)M_{Cu}}{a} \quad (9)$$

$$d_{average} = \frac{6000}{\rho_{Cu}\times S_{Cu}} \quad (10)$$

Where, 2 is a stoichiometric factor, X is the number of moles of N_2O experimentally consumed per unit mass of catalyst (mol g_{cat}^{-1}), N_A is Avogadro's number (6.022×10^{23} mol^{-1}), 1×10^{19} is number of surface Cu atoms per unit surface area (atoms m^{-2}), a is the copper weight percentage in the sample determined by AAS $= m_{Cu}/m_{AC}$ (%), M_{Cu} is the relative atomic mass of copper (63.46 g mol^{-1}).

Catalytic tests

The catalytic reaction was conducted in a fixed-bed flow system described in previous studies.[21,30a] The experimental conditions were as follows: reaction pressure $P = 1.7$ MPa, feed gas $n(CO):n(O_2) = 11/1$, CH_3OH flow rate $= 0.056$ mL min^{-1}, gas hourly space velocity (GHSV) $= 4600$ h^{-1}, and the mass of catalyst (m_{cat}) $=$ 0.25 g. A given mass of catalyst (0.25 g) and quartz sand (40~60 mesh, 3 g) were transferred into a stainless steel tube reactor that had an inner diameter of 6 mm and a length of 450 mm. The addition of quartz sand was to prevent the generation of hotspots in the catalyst bed. The thermocouple was directly inserted into the center of the catalyst bed.[46] Subsequently, methanol (CH_3OH) was pumped through a Series III microfeeder (America Series Co., Ltd.) into a preheater, where it was evaporated and mixed with carbon monoxide (CO) and oxygen (O_2), then entered into the reactor and passed over the catalyst. Flowrates of oxygen and carbon monoxide were set by using mass flow controllers (Beijing Sevenstar Instruments, Inc). Finally, the feed streams of DMC, CH_3OH, dimethoxy methane (DMM), and methyl formate (MF) were injected into the automatic gas sampler (GS-2, Shanghai Sida, China) and were analyzed on-line by using a gas chromatograph (GC-950, Shanghai Haixin, China) equipped with a FID detector. The space time yield (STY, mg g^{-1} h^{-1}), the turnover frequency of DMC (TOF, s^{-1}), and formation rate (rate per unit of Cu surface area, mol m^{-2} s^{-1}) of DMC, were calculated by using Equations (11)–(13):

$$\mathrm{STY} = \frac{m_{\mathrm{DMC}}}{m_{\mathrm{cat}} \times t} = \frac{V_{\mathrm{CH3OH}} \times \rho_{\mathrm{CH3OH}} \times C_{\mathrm{CH3OH}} \times S_{\mathrm{DMC}} \times M_{\mathrm{DMC}}}{2 \times M_{\mathrm{CH3OH}}} \times \frac{1}{m_{\mathrm{cat}} \times t} \quad (11)$$

$$\mathrm{TOF} = \frac{m_{\mathrm{DMC}}}{m_{\mathrm{cat}} \times D_{\mathrm{Cu}} \times t} = \frac{V_{\mathrm{CH_3OH}} \times \rho_{\mathrm{CH_3OH}} \times C_{\mathrm{CH_3OH}} \times S_{\mathrm{DMC}} \times M_{\mathrm{DMC}}}{2 \times M_{\mathrm{CH_3OH}}} \times \frac{1}{m_{\mathrm{cat}} \times D_{\mathrm{Cu}} \times t} \quad (12)$$

$$\mathrm{rate} = \frac{n_{\mathrm{DMC}}}{S_{\mathrm{Cu}} \times t} = \frac{V_{\mathrm{CH_3OH}} \times \rho_{\mathrm{CH_3OH}} \times C_{\mathrm{CH_3OH}} \times S_{\mathrm{DMC}}}{2 \times M_{\mathrm{CH_3OH}}} \times \frac{1}{S_{\mathrm{Cu}} \times t} \quad (13)$$

Where, C_{CH_3OH} is the conversion of CH_3OH (%), S_{DMC} is the selectivity of DMC (%), D_{Cu} is the copper metal dispersion (%), S_{Cu} is the active copper surface area ($m^2 g_{Cu}^{-1}$), V_{CH_3OH} is the flowrate of CH_3OH (0.056 mL min^{-1}), M_{CH_3OH} is the relative atomic mass of CH_3OH (32.04 g mol^{-1}), ρ_{CH_3OH} is the density of CH_3OH (0.7918 g mL^{-1}).

Computational details

All calculations were performed with the Dmol^3 program implemented in the Materials Studio 5.5 package (Accelrys Ltd.). Generalized gradient approximation functionals by Perdew and Wang (PW91) were used to account for the electronic energy of exchange correlation. A polarized split-valence basis set, termed as double numeric polarized basis set, was used. This basis set is comparable in size and quality to the Gaussian G** basis set. The inner electrons of the Cu atoms were kept frozen and were replaced with an effective core potential. Convergence criteria for the optimization of energy, maximum force, and maximum displacement consisted of threshold values of 2×10^{-5} Ha, 0.004 Ha Å^{-1}, and 0.005 Å, respectively. Hence, we set the threshold value for self-consistent field density convergence to 1.0×10^{-5} Ha. To determine accurate activation barriers, the transition states (TSs) for reactions were explored by complete linear synchronous transit/quadratic synchronous transit. In addition, frequency analysis has been used to validate the optimized TS structures, and TS confirmation was performed on every TS structure to confirm that they led to the desired reactants and products.

The equilibrium lattice constant of Cu is $a_{Cu} = 0.3685$ nm, compared with an experimental value of $a_{Cu} = 0.3615$ nm. Good agreement was observed between our computed data and the experimental data reported by Kittel. The substrates are modeled as four atomic layers of metal separated by a vacuum region of 15 Å thickness. The two uppermost substrate layers and reactant molecules are allowed to relax, maintaining the volume constant. A $p(3 \times 3)$ unit cell is adopted for the Cu(111), Cu(220), and Cu(200) surfaces.

Acknowledgements

This work has been supported by grants from the National Natural Science Foundation of China (21376159 and 21276169).

Keywords: Cu(111) · dimethyl carbonate · hollow metal nanoparticles · microwave irradiation · oxidative carbonylation

[1] a) H. Lee, S. E. Habas, S. Kweskin, D. Butcher, G. A. Somorjai, P. Yang, *Angew. Chem Int. Ed.* **2006**, *45*, 7824–7828; *Angew. Chem.* **2006**, *118*, 7988–7992; b) M. A. Mahmoud, C. E. Tabor, M. A. El-Sayed, Y. Ding, Z. L. Wang, *J. Am. Chem. Soc.* **2008**, *130*, 4590–4591.

[2] R. J. Newhouse, H. Wang, J. K. Hensel, D. A. Wheeler, S. Zou, J. Z. Zhang, *J. Phys. Chem. Lett.* **2011**, *2*, 228–235.

[3] a) J.-Y. Gong, S.-H. Yu, H.-S. Qian, L.-B. Luo, X.-M. Liu, *Chem. Mater.* **2006**, *18*, 2012–2015; b) L. Wang, Y. Ebina, K. Takada, T. Sasaki, *Chem. Commun.* **2004**, 1074–1075.

[4] a) K. Kamata, Y. Lu, Y. Xia, *J. Am. Chem. Soc.* **2003**, *125*, 2384–2385; b) D. J. Monk, D. R. Walt, *J. Am. Chem. Soc.* **2004**, *126*, 11416–11417; c) S. Anandhakumar, M. Sasidharan, C.-W. Tsao, A. M. Raichur, *ACS Appl. Mater. Interfaces* **2014**, *6*, 3275–3281.

[5] Z. Bai, L. Yang, L. Li, J. Lv, K. Wang, J. Zhang, *J. Phys. Chem. C* **2009**, *113*, 10568–10573.

[6] H. Djojoputro, X. Zhou, S. Qiao, L. Wang, C. Yu, G. Lu, *J. Am. Chem. Soc.* **2006**, *128*, 6320–6321.

[7] a) L. Wang, T. Sasaki, Y. Ebina, K. Kurashima, M. Watanabe, *Chem. Mater.* **2002**, *14*, 4827–4832; b) F. Caruso, *Chem. Eur. J.* **2000**, *6*, 413–419.

[8] a) Y. Wan, D. Zhao, *Chem. Rev.* **2007**, *107*, 2821–2860; b) X. Zhao, X. Y. Bao, W. Guo, F. Y. Lee, *Mater. Today* **2006**, *9*, 32–39; c) Y. Liu, Y. Chu, Y. Zhuo, L. Dong, L. Li, M. Li, *Adv. Funct. Mater.* **2007**, *17*, 933–938; d) T. He, D. Chen, X. Jiao, Y. Wang, *Adv. Mater.* **2006**, *18*, 1078–1082; e) X. Wang, X. L. Wu, Y. G. Guo, Y. Zhong, X. Cao, Y. Ma, J. Yao, *Adv. Funct. Mater.* **2010**, *20*, 1680–1686; f) Y. Sun, Y. Xia, *Science* **2002**, *298*, 2176–2179; g) H. Woo, B. Mohan, E. Heo, J. C. Park, H. Song, K. H. Park, *Nanoscale Res. Lett.* **2013**, *8*, 390.

[9] J. J. Teo, Y. Chang, H. C. Zeng, *Langmuir* **2006**, *22*, 7369–7377.

[10] Y. Xiong, B. Wiley, J. Chen, Z. Y. Li, Y. Yin, Y. Xia, *Angew. Chem. Int. Ed.* **2005**, *44*, 7913–7917; *Angew. Chem.* **2005**, *117*, 8127–8131.

[11] a) J. Fei, Y. Cui, X. Yan, W. Qi, Y. Yang, K. Wang, Q. He, J. Li, *Adv. Mater.* **2008**, *20*, 452–456; b) H. Cölfen, M. Antonietti, *Angew. Chem. Int. Ed.* **2005**, *44*, 5576–5591; *Angew. Chem.* **2005**, *117*, 5714–5730.

[12] C. E. Fowler, D. Khushalani, S. Mann, *Chem. Commun.* **2001**, 2028–2029.

[13] a) D. Kim, J. Park, K. An, N.-K. Yang, J.-G. Park, T. Hyeon, *J. Am. Chem. Soc.* **2007**, *129*, 5812–5813; b) X. W. Lou, C. Yuan, Q. Zhang, L. A. Archer, *Angew. Chem. Int. Ed.* **2006**, *45*, 3825–3829; *Angew. Chem.* **2006**, *118*, 3909–3913.

[14] C.-Y. Cao, Z.-M. Cui, C.-Q. Chen, W.-G. Song, W. Cai, *J. Phys. Chem. C* **2010**, *114*, 9865–9870.

[15] L. Wang, F. Tang, K. Ozawa, Z. G. Chen, A. Mukherj, Y. Zhu, J. Zou, H. M. Cheng, G. Lu, *Angew. Chem.* **2009**, *121*, 7182–7185.

[16] M. A. Pacheco, C. L. Marshall, *Energy Fuels* **1997**, *11*, 2–29.

[17] N. Keller, G. Rebmann, V. Keller, *J. Mol. Catal. A* **2010**, *317*, 1–18.

[18] a) K. Tomishige, T. Sakaihori, S.-i. Sakai, K. Fujimoto, *Appl. Catal. A* **1999**, *181*, 95 – 102; b) R. Jiang, Y. Wang, X. Zhao, S. Wang, C. Jin, C. Zhang, *J. Mol. Catal. A* **2002**, *185*, 159 – 166.
[19] a) S. King, *J. Catal.* **1996**, *161*, 530 – 538; b) S. King, *Catal. Today* **1997**, *33*, 173 – 182; c) X. Ding, X. Dong, D. Kuang, S. Wang, X. Zhao, Y. Wang, *Chem. Eng. J.* **2014**, *240*, 221 – 227.
[20] M. J. Schneider, M. Haumann, M. Stricker, J. Sundermeyer, P. Wasserscheid, *J. Catal.* **2014**, *309*, 71 – 78.
[21] J. Ren, D. Wang, Y. Pei, Z. Qin, J. Lin, Z. Li, *Chem. J. Chinese U.* **2013**, *34*, 2594 – 2600.
[22] J. Ren, W. Wang, D. Wang, Z. Zuo, J. Lin, Z. Li, *Appl. Catal. A* **2014**, *472*, 47 – 52.
[23] Q. Hua, T. Cao, X. K. Gu, J. Lu, Z. Jiang, X. Pan, L. Luo, W. X. Li, W. Huang, *Angew. Chem. Int. Ed.* **2014**, *53*, 4856 – 4861; *Angew. Chem.* **2014**, *126*, 4956 – 4961.
[24] S. A. Anderson, T. W. Root, *J. Catal.* **2003**, *217*, 396 – 405.
[25] a) B. Wang, H. B. Wu, L. Zhang, X. W. D. Lou, *Angew. Chem. Int. Ed.* **2013**, *52*, 4165 – 4168; *Angew. Chem.* **2013**, *125*, 4259 – 4262; b) J. Ren, M. Ren, D. Wang, J. Lin, Z. Li, *J. Therm. Anal. Calorim.* **2015**, *120*, 1929 – 1939.
[26] F. Wang, A. Kalam, L. Chang, D. Xie, A. S. Al-Shihri, G. Du, *Mater. Lett.* **2013**, *92*, 96 – 99.
[27] a) W. Yu, B. Yang, X. Chen, W. Jiang, Q. Yu, B. Xu, *Vacuum* **2012**, *86*, 2005 – 2009; b) D. Vennerberg, R. Quirino, M. R. Kessler, *Adv. Eng. Mater.* **2013**, *15*, 366 – 372; c) J. Bian, X. Wei, Y. Jin, L. Wang, D. Luan, Z. Guan, *Chem. Eng. J.* **2010**, *165*, 686 – 692.
[28] H. G. Yang, H. C. Zeng, *J. Phys. Chem. B* **2004**, *108*, 3492 – 3495.
[29] R. L. Moss, D. Pope, B. Davis, D. Edwards, *J. Catal.* **1979**, *58*, 206 – 219.
[30] a) J. Ren, C. Guo, L. Yang, Z. Li, *Chin. J. Catal.* **2013**, *34*, 1734 – 1744; b) D. Liang, J. Gao, J. Wang, P. Chen, Z. Hou, X. Zheng, *Catal. Commun.* **2009**, *10*, 1586 – 1590.
[31] A.-X. Wang, D.-Q. Chu, L.-M. Wang, B.-G. Mao, H.-M. Sun, Z.-C. Ma, *RSC Adv.* **2014**, *4*, 7545 – 7548.
[32] a) Y. Zhang, D. N. Briggs, E. de Smit, A. T. Bell, *J. Catal.* **2007**, *251*, 443 – 452; b) M. S. Han, B. G. Lee, B. S. Ahn, D. J. Moon, S. I. Hong, *Appl. Surf. Sci.* **2003**, *211*, 76 – 81.
[33] Z.-J. Zuo, W. Huang, P.-D. Han, Z.-H. Li, *Acta Phys. Chim. Sin.* **2009**, *25*, 2507 – 2512.
[34] Y. Zhang, A. T. Bell, *J. Catal.* **2008**, *255*, 153 – 161.
[35] G. Zhang, Z. Li, H. Zheng, T. Fu, Y. Ju, Y. Wang, *Appl. Catal. B* **2015**, *179*, 95 – 105.
[36] B. Yan, S. Huang, S. Wang, X. Ma, *ChemCatChem* **2014**, *6*, 2671 – 2679.
[37] G. Merza, B. László, A. Oszkó, G. Pótári, K. Baán, A. Erdőhelyi, *J. Mol. Catal. A* **2014**, *393*, 117 – 124.
[38] Z. Li, K. Xie, R. C. T. Slade, *Appl. Catal. A* **2001**, *205*, 85 – 92.
[39] M. Komarneni, J. Shan, A. Chakradhar, E. Kadossov, S. Cabrini, U. Burghaus, *J. Phys. Chem. C* **2012**, *116*, 5792 – 5801.
[40] J. Zhou, H. Song, X. Chen, L. Zhi, J. Huo, B. Cheng, *Chem. Mater.* **2009**, *21*, 3730 – 3737.
[41] Y. Han, H. Wang, M. Zhang, M. Su, W. Li, K. Tao, *Inorg. Chem.* **2008**, *47*, 1261 – 1263.
[42] a) X. W. D. Lou, L. A. Archer, Z. Yang, *Adv. Mater.* **2008**, *20*, 3987 – 4019; b) X. W. Lou, Y. Wang, C. Yuan, J. Y. Lee, L. A. Archer, *Adv. Mater.* **2006**, *18*, 2325 – 2329; c) M. Choi, K. Na, J. Kim, Y. Sakamoto, O. Terasaki, R. Ryoo, *Nature* **2009**, *461*, 246 – 249; d) R. Qiao, X. L. Zhang, R. Qiu, J. C. Kim, Y. S. Kang, *Chem. Mater.* **2007**, *19*, 6485 – 6491; e) J. H. Pan, X. Zhang, A. J. Du, D. D. Sun, J. O. Leckie, *J. Am. Chem. Soc.* **2008**, *130*, 11256 – 11257.
[43] a) A. Mahapatra, U. Bhatta, T. Som, *J. Phys. D* **2012**, *45*, 415303; b) Y. Deng, H. Wang, L. Xu, Y. Wu, C. Zhong, W. Hu, *RSC Adv.* **2013**, *3*, 4666 – 4672.
[44] J. Liu, D. Xue, *Adv. Mater.* **2008**, *20*, 2622 – 2627.
[45] P. Munnik, M. Wolters, A. Gabrielsson, S. Pollington, G. Headdock, J. Bitter, P. De Jongh, K. De Jong, *J. Phys. Chem. C* **2011**, *115*, 14698 – 14706.
[46] K. Takehira, T. Shishido, *Catal. Surv. Asia* **2007**, *11*, 1 – 30.

Received: October 29, 2015
Published online on January 28, 2016